electronics

MDPI

Article

Wavelet Analysis to Detect Ground Faults in Electrical Power Systems with Full Penetration of Converter Interface Generation

Luis Santiago Azuara Grande [1,*], Ricardo Granizo [2] and Santiago Arnaltes [1]

[1] Electrical Engineering Department, Universidad Carlos III de Madrid, 28911 Leganes, Spain
[2] Electric, Electronic, Automatic and Applied Physics Department, ETSIDI, Universidad Politécnica de Madrid, 28012 Madrid, Spain
* Correspondence: lazuara@ing.uc3m.es

Abstract: The requirements for the increased penetration of renewable energy sources in electrical power systems have led to a dominance of power electronic interfaces. As a result, short-circuit currents have been reduced by the thermal limitations of power electronics, leading to problems associated with the sensitivity, selectivity, and reliability of protective relays. Although many solutions can be found in the literature, these depend on communications and are not reliable in all grid topologies or under different types of electrical fault. Hence, in this paper, the analysis of ground fault currents and voltages using a wavelet transform in combination with a new algorithm not only detects such ground faults but also allows them to be cleared quickly and selectively in scenarios with low fault current contribution due to a full penetration converter-interface-based generation. To verify and validate the proposed protection system, different ground faults are simulated using an arc ground fault model in a grid scheme based on the IEEE nine-bus standard test system, with only grid-forming power converters as generation sources. The test system is modelled in the MATLAB/Simulink environment. Therefore, the protection relays that verify all the steps established in the new algorithm can detect and clear any ground defect. Simulations are also presented involving different fault locations to demonstrate the effectiveness of the proposed ground fault protection method.

Keywords: grid-forming power converter; wavelet transform; renewable energy sources; electrical faults; fault detection; arc ground faults

Citation: Azuara Grande, L.S.; Granizo, R.; Arnaltes, S. Wavelet Analysis to Detect Ground Faults in Electrical Power Systems with Full Penetration of Converter Interface Generation. *Electronics* **2023**, *12*, 1085. https://doi.org/10.3390/electronics12051085

Academic Editors: M. Tariq Iqbal, Giovanna Adinolfi, Maria Valenti and Giorgio Graditi

Received: 2 February 2023
Revised: 15 February 2023
Accepted: 20 February 2023
Published: 22 February 2023

1. Introduction

Highly volatile fuel prices, stringent energy security requirements and climate change have driven the growth in the use of renewable energy sources in electrical power systems. Most renewable energy sources require power electronic interfaces, i.e., converters, as wind and solar generation are the most common forms [1]. Due to the high penetration requirements of renewable energy sources, power electronics play an important role in ensuring the stability and performance of electrical power systems [2]. However, new challenges have also arisen, and particularly in connection with protection systems to detect electrical faults [3].

To protect the semiconductor switches of the converters, current limiters are included that maintain the fault current level below the maximum design value [4]. The fault current that is delivered depends on the design parameters, which differs from one converter to the next and between manufacturers. The control of the converter and the thermal capacity of the semiconductor switches are also important factors affecting the magnitude of the fault current [5].

Due to the thermal restrictions on semiconductor switches, converters are designed to limit the maximum current to 1–2 p.u. of the rated current, unlike synchronous generators, which can provide a short-circuit current of up to 5–8 p.u. of the rated current [6].

Overcurrent protective relays are the most widespread protection in its application, and they need a minimum amount of current to operate. Converter-based generators

cannot supply a level of short-circuit current that is higher than required by the protective relay [7]. The design of overcurrent protection relays for small fault currents can cause nuisance tripping [5]. There is, therefore, a need to develop new protection techniques. The literature contains numerous proposals for protection systems, and some of these are reviewed below.

Voltage-based detection techniques, as proposed in [8–10], can be used to identify faults with low current levels, since any fault causes a drop in the grid voltage. When the voltage signal measurement is lower than the allowed value of the voltage drop, the protection relay trips [11]. The main disadvantage of voltage-based protection methods is that any voltage drop in the grid can cause the unnecessary tripping of the protection relay. The protection also cannot recognize high-impedance faults, and this technique is designed for grids with specific characteristics, meaning that it depends on the grid configuration and may not be suitable for grids with multiple configurations [12].

Another approach [13,14] is to use energy storage systems (e.g., flywheels, supercapacitors, etc.) with high short-circuit capabilities to increase the fault current supplied. Although this allows for the implementation of conventional overcurrent protection, the high costs involved rule out its implementation.

Differential protection is another common method and was presented in [15–17]. In this method, the currents entering and leaving the protected zone are compared, and the protection system only operates when the difference between these currents is greater than a pre-set threshold. This scheme requires protective relays at each end of the line, which increases the cost. In addition, a communication infrastructure is required to send current measurements from both ends of the line, which also increases the cost and compromises the safety of the protection system. Furthermore, measurements need to be synchronized. Finally, unbalanced loads and transients can lead to protection failure [11].

To detect and isolate faulty areas in the grid, the distance protection strategy presented in [18] mainly relies on admittance or impedance measurements. Normally, distance protection does not require communication between relays [19]. However, the distance protection scheme has several drawbacks, such as problems with measurement accuracy due to the presence of harmonics, inaccuracy in the admittance measurement due to fault resistance, and the difficulty of measuring impedance/admittance in short lines [12].

The proposals in the literature have significant disadvantages associated with the protection of future grids. Currently, a grid protection strategy is sought that is not dependent on communications, and that is reliable in any grid topology (grid-connected, isolated, with synchronous generation or power electronic interfaces) and under different types of electrical fault (phase-to-ground, arc faults, high-impedance faults, etc.).

In addition, the performance of protections for detecting ground faults based on line differential, distance and overcurrent schemes are quite different from the performance of the scheme proposed in this paper. A line differential method uses different algorithms to stabilize its actuation under through faults. Such algorithms detect different levels of harmonics, and the tripping characteristic is then shifted accordingly as a function of the severity of these harmonics. This type of protection normally relies on a dynamic change in the setting of the tripping curve stabilization current versus the differential current to determine whether to trip or not. In the distance protection, the zero-compensation factor needs to be defined to achieve good performance. In this kind of protection, the negative sequence components are evaluated to trigger its actuation. Overcurrent protection schemes evaluate the value of the current using harmonic filters to assess mainly the fundamental, second and fifth harmonic levels, and then take a decision on whether or not to trip as a function of these settings [20].

The novel contribution of this research is the application of wavelet transform analysis to detect ground faults in a generation scenario of 100% converter interface penetration without synchronous generators, which will be the trend in future electrical power systems. The Daubechies mother wavelet is used to obtain the values of the detail coefficients to selectively detect any ground fault, regardless of the values relied on by traditional

protection schemes. This research also demonstrates the performance of the suggested technique through a complete simulation of arcing faults in a grid with 100% renewable energy sources based on power electronic interfaces. All the components involved in the study were modelled in the MATLAB/Simulink environment, including the control of the grid-forming converter.

This paper is organized as follows: Section 2 presents the grid model along with its specifications. In Section 3, the grid-forming VSC control and its current limit strategy are introduced. Section 4 describes the arc ground fault using the Cassie model. In Section 5, a wavelet transform analysis is proposed for the detection of faults with low current levels. Section 6 explains the operational sequence of the protection relay algorithm. Section 7 presents and discusses some results. Finally, conclusions are given in Section 8.

2. Grid Model

A 50 Hz grid model has been outlined using the standard IEEE nine-bus test system, as illustrated in Figure 1, in which the synchronous generators are replaced by grid-forming voltage source converters (VSCs). The positions of the protection relays, transmission lines and the main transformer specifications can also be found in Figure 1. The shunt admittance (Y) and the series impedance (Z) are expressed in per unit (p.u.) values with a $S_{base} = 100$ MVA and a $V_{base} = 230$ kV.

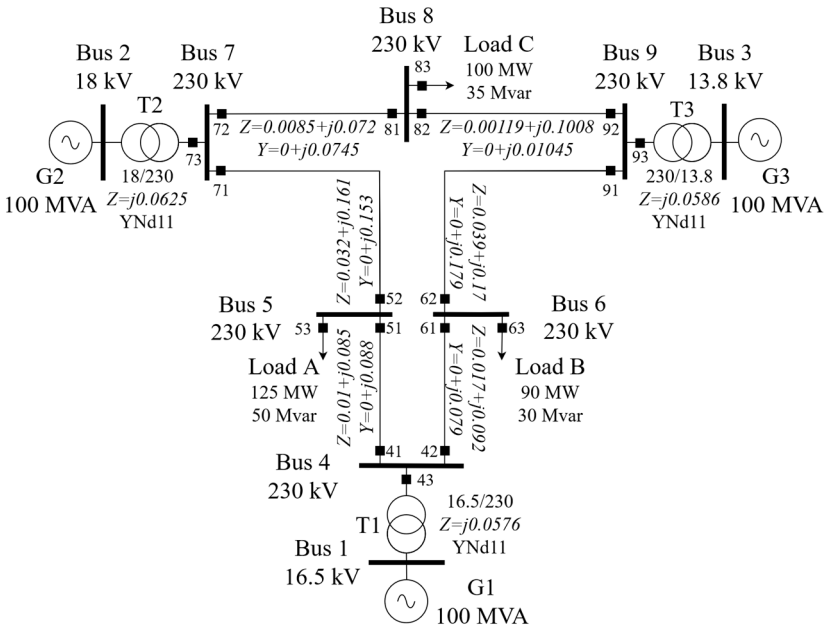

Figure 1. Standard IEEE nine-bus test system.

Three grid-forming VSCs rated at 100 MVA are connected to buses 1, 2, and 3, and three loads, modelled as constant impedances, are connected to buses 5, 6, and 8, for which the specifications are given in Figure 1. The electric grid and the generators are connected through three MV/HV transformers, which are modelled as a three-phase linear transformer. The electric grid has six transmission lines, modelled by a nominal π section, and nine buses.

3. Grid-Forming VSC Control

An analysis of grid-forming VSC control is essential, as the generation units with converter interfaces are the only generators in the grid evaluated here and play a key role in the fault behavior. A grid-forming VSC control has been modelled together with the IEEE nine-bus system, to study and verify the proposed detection fault strategy.

3.1. Grid-Forming VSC Cascaded Control Scheme

Figure 2 shows the cascaded control scheme of the grid-forming VSC with the inner voltage and current control loops, which are realized in the synchronous rotating frame (dq), together with the cross-coupling and feed-forward terms. The current references are determined by the voltage loop. They are then passed to the current loop, which produces the modulated voltage for the linearization stage. Finally, the modulation signals are sent to the switching stage of the power converter. An outer control based on the P-f droop control determines the control angle θ by the integral of the angular frequency as shown in (1), and another based on the Q-V droop control gives the voltage reference e^*_{gd}, as shown in (2). The primary control is represented by the equations below [21,22]:

$$\omega^* = \omega_{set} + m_p(P^* - P_{mes}) \tag{1}$$

$$e^*_{gd} = V_{set} + m_q(Q^* - Q_{mes}) \tag{2}$$

where the active power reference and the output are given by P^* and P_{mes}, respectively; the angular frequency output reference and the set value are given by ω^* and ω_{set}, respectively; m_p is the active power droop gain; the reactive power reference and the output are given by Q^* and Q_{mes}; e^*_{gd} is the voltage reference; V_{set} is the set voltage value of reactive power droop; and m_q is the reactive power droop gain.

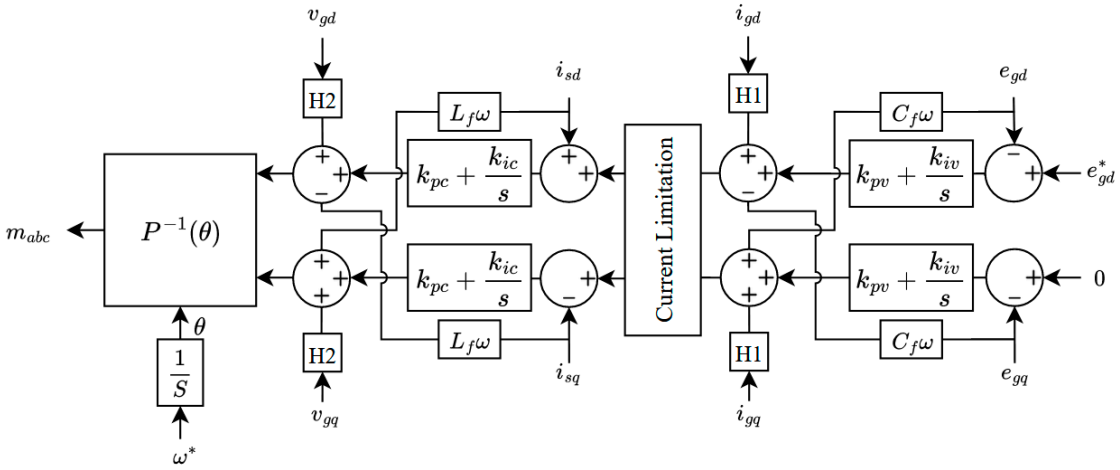

Figure 2. Cascaded control scheme for the grid-forming VSC [21].

The p.u. parameters of the grid-forming VSC used in MATLAB/Simulink simulations are provided in Table 1.

Table 1. Grid-forming VSC parameters (in p.u).

Parameter	Value	Parameter	Value	Parameter	Value
L_f	0.2	R_f	0.01	C_f	0.2
k_{ic}	160	k_{pc}	2	H1	0.75
k_{iv}	7.8	k_{pv}	1	H2	1

Where k_{pc} and k_{ic} are proportional and integral gains of the current controller, respectively; k_{pv} and k_{iv} are the proportional and integral gains of the voltage controller, respectively; C_f, L_f and R_f are the filter capacitance, inductance, and resistance, respectively; and the gains H1 and H2 reduce the disturbances introduced into the control.

A current limitation strategy was also designed to prevent damage to the VSC due to overcurrent. This strategy must be included in the control scheme of the converter in order to achieve the main objective of protecting the semiconductor switches. In the following sections, the current limiting strategy is explained.

3.2. Current Limit Strategy

The main objectives are to keep all components of the converter within their rated values and to avoid overcurrent during transient events. By setting the limiting current between the two inner loop controllers, as shown in the Current Limitation block in Figure 2, the reference switching current is limited and its dq components are constrained by vector amplitude saturation [23].

This method requires calculating the current reference amplitude $\left|\overline{I^*_{dq}}\right|$ and the vector angle δ_{dq} resulting from the DQ components using the following equations [23]:

$$\left|\overline{I^*_{dq}}\right| = \sqrt{\left(I^*_d\right)^2 + \left(I^*_q\right)^2} \tag{3}$$

$$\delta_{dq} = \tan^{-1}\left(\frac{I^*_q}{I^*_d}\right) \tag{4}$$

The absolute value of the reference current amplitude $\left|\overline{I^*_{dq}}\right|$ can be limited. The current amplitude can be determined and limited according to the ability of the converter components to handle the overcurrent, as shown in Figure 3. The angle is also required to calculate the saturated values of each current component. Thus, in the same way as a synchronous generator, the grid-forming VSC can give a grid-impedance-dependent P/Q ratio in the event of a fault [23]. Since a limiting value of $I_{max} = 2$ p.u. is set, the converter can supply a certain amount of overcurrent in the case of a fault.

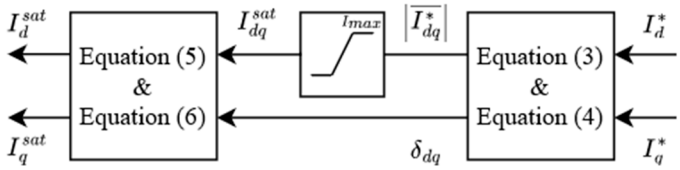

Figure 3. Implementation of vector amplitude saturation [23].

Where [23]:

$$I_d^{sat} = cos\ \left(\delta_{dq}\right) \cdot I_{dq}^{sat} \tag{5}$$

$$I_q^{sat} = \sin\left(\delta_{dq}\right) \cdot I_{dq}^{sat} \tag{6}$$

4. Arc Grounding Fault Model

Most short-circuits in electrical power systems are ground faults; the most common of these are arcing faults, and the investigation of short-circuit faults shows that these represent more than 80% of the total [24].

The simulation of arcing models makes it possible to better understand the arcing events that appear in high-voltage electrical power systems. The three mathematical models of arcing are physical models, black box models, and parameter models, as described below [25].

4.1. Physical Models

These are based on fluid dynamics rules, such as the laws of thermodynamics in conjunction with Maxwell's equations and involve complicated mathematics.

4.2. Black Box Models

These describe the behavior of the arc and are used to simulate arc-circuit interactions. The arc is described through one or more differential equations relating its conductance to the circuit variables, such as the arc voltage and arc current.

4.3. Parameter Models

These are more precise than black box models, but their parameters are acquired from complex equations and tables.

Since the internal conditions of the arc are very complex, a black box model is often used to characterize the arc in order to better understand its electrical characteristics. The Cassie model is a classic example, and gives good results for arcs with high currents [25]. Therefore, the Cassie model was implemented in the IEEE nine-bus system to simulate an arcing fault and to analyze the proposed detection strategy in a more realistic way.

Cassie assumed that power losses occur only through convection, which implies that the temperature in the arc remains constant. As a result, the cross-sectional area of the arc is proportional to the current, and the voltage across the arc is constant [25]. The Cassie arc model represents the dynamic properties of an arc.

5. Wavelet Transform Analysis

Fourier analysis is a standard method for analyzing a time-domain waveform in the frequency domain [26]. When obtaining the Fourier transform of a signal with transients, one of the difficulties of this approach becomes apparent. The Fourier transform of the signal is evaluated at a given frequency using a weighted average over the entire period, and since a transient form only a very small part of the total time duration of the signal, its contribution to the frequency domain representation of the signal may be negligible compared to the contribution from the rest of the signal [27]. Consequently, it is difficult to identify the prominent frequency features of signal transients using a frequency domain representation [28]. In addition, the representation of the signal in the frequency domain does not provide information about the timing of the transients. As a result, the Fourier transform lacks a multi-resolution representation in terms of both time and frequency [29].

In contrast to the Fourier method, the wavelet transform offers both time and frequency localization [30]. This makes it possible to identify and evaluate the transients that can occur in electrical power systems [31]. Using wavelet coefficients, faults can be detected, since during transients they reach the maximum value of the modulus [32]. Thus, whether the coefficients exceed the established thresholds, a discrimination between faults and the nominal values of the electrical power system can be perfectly performed.

The wavelet transform can be used to extract information from a transient signal in the time domain by decomposing the signal into a high-frequency band with a short window scale and a low-frequency band with a long window scale, as opposed to the Fourier transform. This makes it particularly effective for analyzing signals with harmonics using the discrete wavelet transform (DWT), as seen in Equation (7) [33].

$$DWT(s,m,k) = \frac{1}{\sqrt{a}} \sum_{n} s(n) \Psi^* \left(\frac{k-b}{a} \right) \tag{7}$$

where $s(n)$ is the input signal to be decomposed, Ψ is the mother wavelet, and the scaling and translation parameters $a = a_0^m$ and $b = na_0^m$ respectively, are functions of integer parameter m.

The mother wavelet that is developed for the wavelet transform analysis must perform well in extracting the primary properties of the input signal as well as having appropriate harmonic removal features [20]. There are several mother wavelets such as Haar, Daubechies, Biorthogonal, Coiflets, etc.

Depending on the sampling frequency of the original signal, the number of decomposition steps is determined. The first decomposition has two elements: a high-frequency element D1 and a low-frequency element A1. As a function of the sampling frequency f_s, the frequency band of D1 element is $f_s/2 - f_s/4$ Hz, whereas the frequency band of A1 element is $f_s/4 - 0$ Hz. In the second decomposition, the A1 element is decomposed into D2 element for the high-frequency band ($f_s/4 - f_s/8$ Hz) and A2 element for the low-frequency band ($f_s/8 - 0$ Hz) [34].

This procedure is repeated until the appropriate frequency band is attained and the proper information can be retrieved from the assessed signal. In Figure 4, the decomposition developed by the DWT can be seen. A and D represent the approximation and detail coefficients, respectively [35].

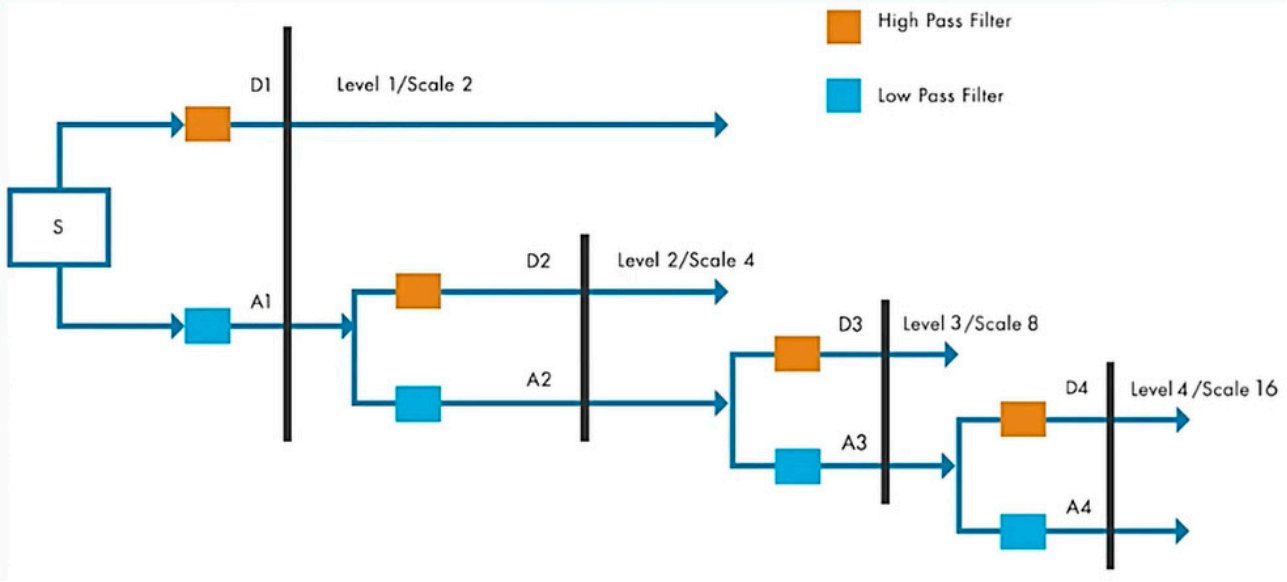

Figure 4. Frequency bands of the discrete wavelet transform related to decomposition steps [35].

In this paper, a wavelet transform analysis is applied to the voltage and current waveforms, using the wavelet toolbox in MATLAB, with the one-dimensional multi-scale technique to detect faults in electrical power systems with 100% renewable energy sources based on power electronic interfaces.

6. Protection Relay Algorithm

The sequence of operation of the proposed fault detection method is illustrated in Figure 5, which shows the steps to be carried out by the protection algorithm at each of the 18 relays included in the standard IEEE nine-bus test system.

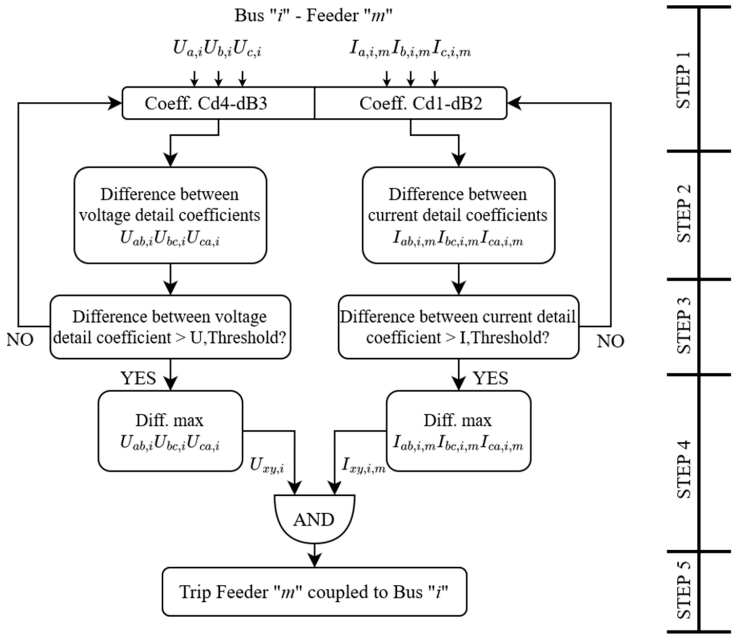

Figure 5. Flowchart of the operational sequence of the protection relay.

The operational sequence consists of five steps that are explained below:

- Step 1: measure the three-phase voltage waveform for bus i and the current waveform for a feeder m coupled to bus i, and calculate their voltage and current detail coefficients by applying the wavelet transform.
- Step 2: calculate the values $U_{ab,i}$, $U_{bc,i}$ and $U_{ca,i}$ as the differences between the voltage detail coefficients, i.e., as $U_{ab,i} = U_{a,i} - U_{b,i}$, $U_{bc,i} = U_{b,i} - U_{c,i}$ and $U_{ca,i} = U_{c,i} - U_{a,i}$, and calculate the values $I_{ab,i,m}$, $I_{bc,i,m}$ and $I_{ca,i,m}$ as the differences between the current detail coefficients, i.e., as $I_{ab,i,m} = I_{a,i,m} - I_{b,i,m}$, $I_{bc,i,m} = I_{b,i,m} - I_{c,i,m}$ and $I_{ca,i,m} = I_{c,i,m} - I_{a,i,m}$.
- Step 3: Check whether the differences between the voltage detail coefficients and current detail coefficients obtained in Step 2 are higher than the voltage threshold value and the current threshold value, respectively. Such thresholds are taken as half of the maximum values of the detail coefficient for voltages and currents.
- Step 4: check whether the maximum differences between the voltage detail coefficients and current detail coefficients that have exceeded their established thresholds have the same phase sub-index x and y, i.e., $U_{ab,i}$ and $I_{ab,i,m}$, $U_{bc,i}$ and $I_{bc,i,m}$, or $U_{ca,i}$ and $I_{ca,i,m}$.
- Step 5: Trip feeder m coupled to bus i.

7. Results

To verify the correct performance of the wavelet transform analysis in terms of detecting ground faults in grids with the full penetration of renewable energies based on power electronic interfaces, three arc faults (phase-to-ground) were simulated for the instant t = 3.95 s at different locations of the grid. The first was in phase A at load A, the second in phase B on the transmission line from bus 4 to bus 6, and the third in phase C on the transmission line from bus 8 to bus 9.

The waveforms of the voltage and current were analyzed for all the protection relays of the IEEE nine-bus system using the Daubechies mother wavelets dB3 and dB2, respectively. The choice of mother wavelet will depend on the type of signal to be analyzed and the information to be obtained from it. In particular, for the analysis of electrical power systems, the Daubechies family gives the most suitable and reliable results, in addition to outstanding performance in the detection of waveform discontinuities [36,37]. Since the behavior of the voltage and current waveforms is not the same during a fault event, it is necessary to use signal decompositions at different scales. Fast and short transient disturbances will be detected at lower scales (dB2), while slower, longer transient disturbances will be detected at higher scales (dB10) [38].

The threshold values of the protection relays for the detail coefficients were also set based on the results obtained in the multiple simulation studies performed on the IEEE nine-bus test system. Since every electrical power system has different configurations and buses, the thresholds must be studied for each, and this is carried out for all protection systems.

7.1. Fault at Load A

A phase-to-ground arc fault was simulated in phase A at load A of the grid model. The three-phase voltage and current waveforms during the fault are illustrated in Figure 6. The voltage in the faulty phase was reduced to the arcing voltage at the same instant as the fault occurs, while the current in the faulty phase was increased to 2 p.u. Hence, the amount of current was not high enough to reach the tripping threshold of the protection, as the difference from the rated current was insufficient.

To detect faults, the voltage and current waveforms measured at the protection relays were decomposed using wavelet transform analysis up to level 4 with dB3, and up to level 1 with dB2. Figure 6 shows the wavelet coefficients of the current and voltage in phase A, which show very fast detection of the disturbance generated by the fault, within the range of one and a half cycles. The results of the simulation with all the values of the detail coefficients for the voltage and current phases at each protection relay during the phase-to-ground arc fault are listed in Table 2.

Based on the results in Table 2, the protection algorithm illustrated in the scheme in Figure 5 was executed. We obtained the differences in the voltage and current detail coefficients

between the phases (i.e., A–B, B–C, and C–A) and compared them with the threshold values. The voltage threshold was set to 0.15 and current threshold was set to 1.9. Figures 7 and 8 show the results of the protection algorithm, and it can be seen that the differences in the voltage and current detail coefficients clearly indicate the location of the fault.

In Figures 7 and 8, relays 51, 52 and 53 exceeded the thresholds established in the protection algorithm. Only relay 53 was tripped, as it had the largest difference between the current detail coefficients of the bus. The fault was, therefore, cleared correctly, with selectivity and without sensitivity problems.

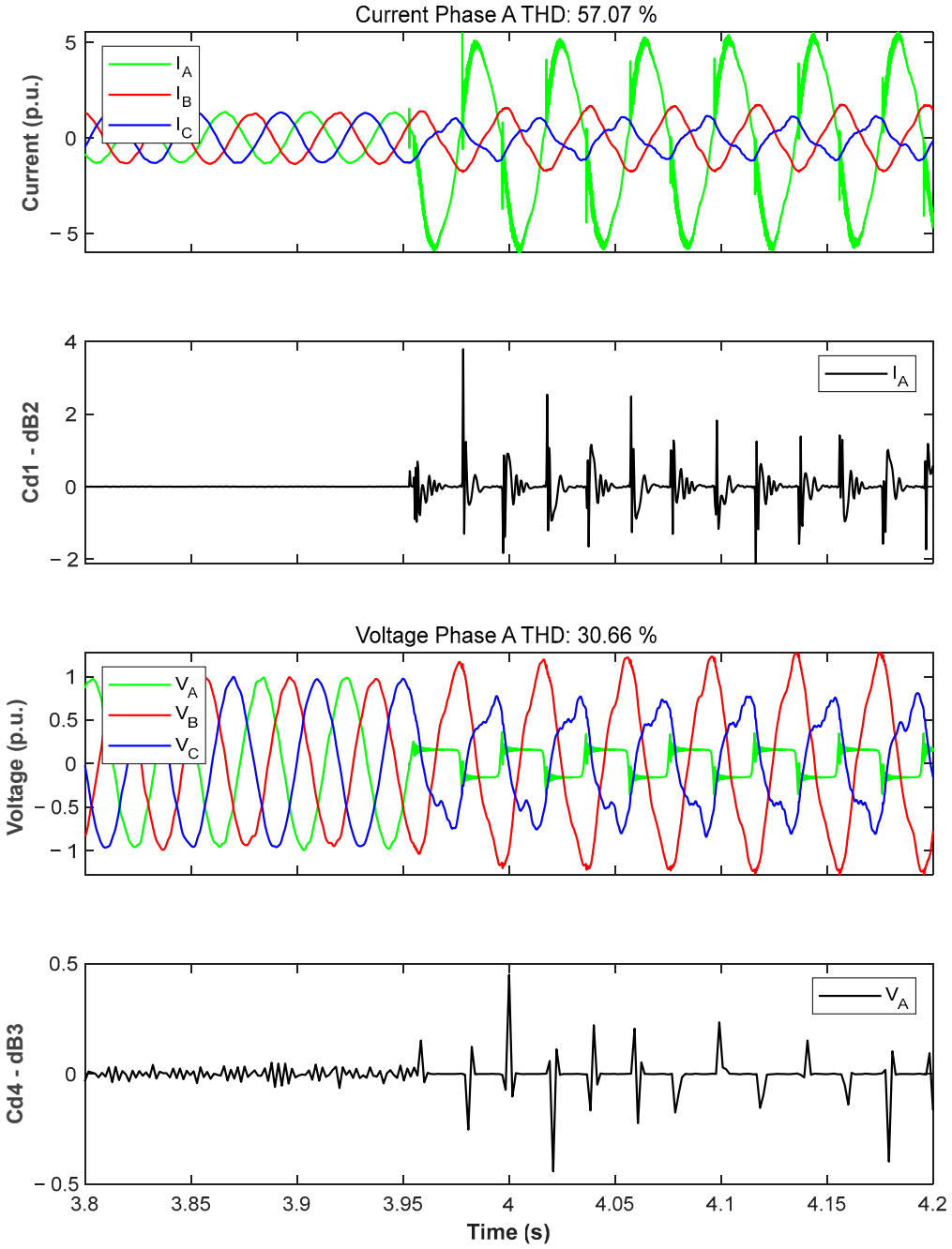

Figure 6. Three-phase currents and voltages and the Wavelet coefficients for the current and voltage in phase A during a phase-to-ground arc fault at the fault location (i.e., on the load side).

Table 2. Detail coefficients during phase-to-ground arc fault at load A.

Relay No.	Detail Coefficients					
	Voltage (Cd4–dB3)			Current (Cd1–dB2)		
	Phase A	Phase B	Phase C	Phase A	Phase B	Phase C
41	2.58×10^{-1}	1.42×10^{-1}	1.45×10^{-1}	1.78×10^{-2}	1.02×10^{-2}	1.26×10^{-2}
42	2.58×10^{-1}	1.42×10^{-1}	1.45×10^{-1}	1.63×10^{-2}	9.40×10^{-3}	1.36×10^{-2}
43	2.58×10^{-1}	1.42×10^{-1}	1.45×10^{-1}	8.10×10^{-3}	1.71×10^{-2}	8.70×10^{-3}
51	4.08×10^{-1}	1.02×10^{-1}	9.92×10^{-2}	1.44	8.90×10^{-3}	1.01×10^{-2}
52	4.08×10^{-1}	1.02×10^{-1}	9.92×10^{-2}	2.41	1.73×10^{-2}	1.72×10^{-2}
53	4.08×10^{-1}	1.02×10^{-1}	9.92×10^{-2}	3.78	2.76×10^{-2}	2.59×10^{-2}
61	1.66×10^{-1}	1.07×10^{-1}	9.97×10^{-2}	5.50×10^{-3}	3.60×10^{-3}	4.00×10^{-3}
62	1.66×10^{-1}	1.07×10^{-1}	9.97×10^{-2}	5.50×10^{-3}	2.70×10^{-3}	5.20×10^{-3}
63	1.66×10^{-1}	1.07×10^{-1}	9.97×10^{-2}	1.80×10^{-3}	9.92×10^{-4}	8.50×10^{-3}
71	1.62×10^{-1}	1.56×10^{-1}	1.51×10^{-1}	8.30×10^{-3}	8.30×10^{-3}	1.48×10^{-2}
72	1.62×10^{-1}	1.56×10^{-1}	1.51×10^{-1}	3.40×10^{-3}	2.80×10^{-3}	2.70×10^{-3}
73	1.62×10^{-1}	1.56×10^{-1}	1.51×10^{-1}	1.64×10^{-2}	1.06×10^{-2}	1.15×10^{-2}
81	1.56×10^{-1}	1.28×10^{-1}	1.89×10^{-1}	2.50×10^{-3}	5.20×10^{-3}	2.40×10^{-3}
82	1.56×10^{-1}	1.28×10^{-1}	1.89×10^{-1}	1.06×10^{-2}	4.50×10^{-3}	2.20×10^{-3}
83	1.56×10^{-1}	1.28×10^{-1}	1.89×10^{-1}	2.70×10^{-3}	1.80×10^{-3}	9.20×10^{-3}
91	1.58×10^{-1}	1.70×10^{-1}	1.89×10^{-1}	3.30×10^{-3}	3.60×10^{-3}	8.10×10^{-3}
92	1.58×10^{-1}	1.70×10^{-1}	1.89×10^{-1}	2.70×10^{-3}	4.60×10^{-3}	1.60×10^{-3}
93	1.58×10^{-1}	1.70×10^{-1}	1.89×10^{-1}	6.10×10^{-3}	1.07×10^{-2}	4.30×10^{-3}

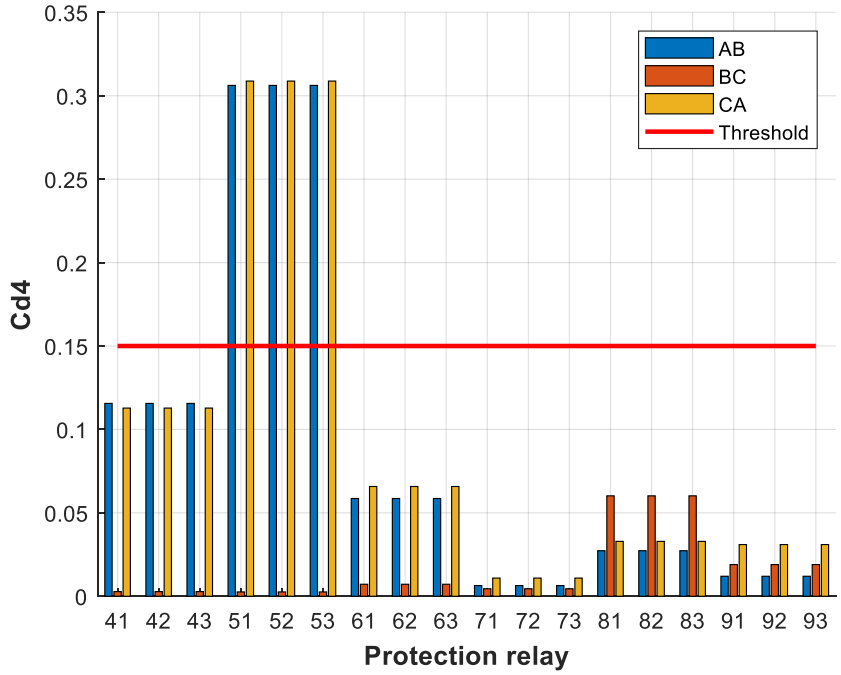

Figure 7. Differences in the voltage Cd4-dB3 at load A.

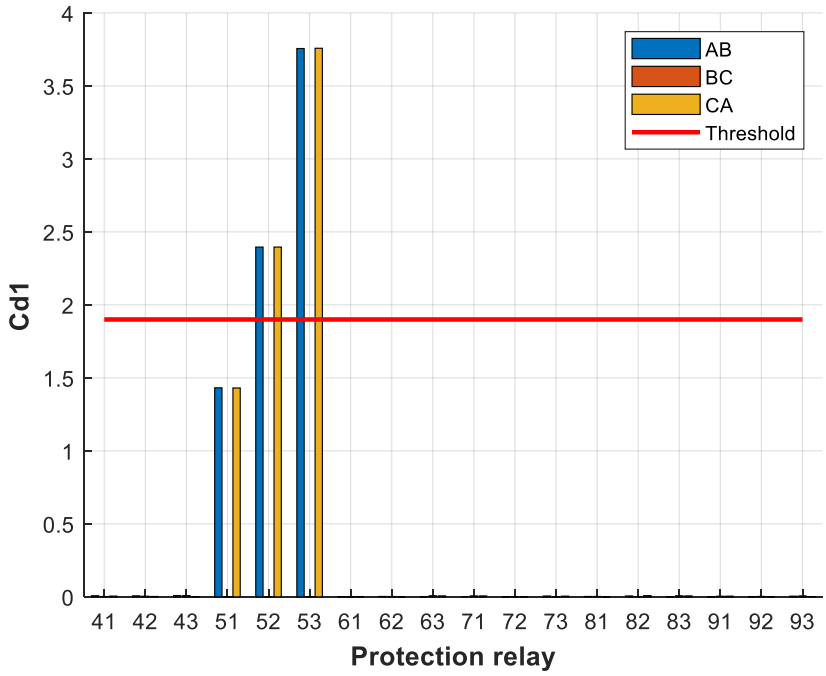

Figure 8. Differences in the current detail Cd1-dB2 at load A.

7.2. Fault on Transmission Line from Bus 4 to Bus 6

In this case, a phase-to-ground arc fault was simulated in phase B, on the transmission line from bus 4 to bus 6 of the grid model. Table 3 shows all the values of the detail coefficients obtained for the voltage and current phases at each protection relay during the fault.

Table 3. Detail coefficients during phase-to-ground arc fault at transmission line from bus 4 to bus 6.

Relay No.	Detail Coefficients					
	Voltage (Cd4–dB3)			Current (Cd1–dB2)		
	Phase A	Phase B	Phase C	Phase A	Phase B	Phase C
41	2.39×10^{-1}	4.68×10^{-1}	1.91×10^{-1}	8.90×10^{-3}	2.16×10^{-2}	8.70×10^{-3}
42	2.39×10^{-1}	4.68×10^{-1}	1.91×10^{-1}	4.50×10^{-3}	4.25×10^{-2}	5.90×10^{-3}
43	2.39×10^{-1}	4.68×10^{-1}	1.91×10^{-1}	1.06×10^{-2}	1.43×10^{-2}	8.70×10^{-3}
51	6.42×10^{-2}	1.26×10^{-1}	9.92×10^{-2}	3.00×10^{-3}	5.20×10^{-3}	2.50×10^{-3}
52	6.42×10^{-2}	1.26×10^{-1}	9.92×10^{-2}	2.20×10^{-3}	4.60×10^{-3}	5.90×10^{-3}
53	6.42×10^{-2}	1.26×10^{-1}	9.92×10^{-2}	1.80×10^{-3}	3.70×10^{-3}	7.10×10^{-3}
61	1.01×10^{-1}	3.75×10^{-1}	1.50×10^{-1}	9.70×10^{-3}	3.65×10^{-2}	1.05×10^{-2}
62	1.01×10^{-1}	3.75×10^{-1}	1.50×10^{-1}	1.05×10^{-2}	3.44×10^{-2}	1.02×10^{-2}
63	1.01×10^{-1}	3.75×10^{-1}	1.50×10^{-1}	2.90×10^{-3}	1.18×10^{-2}	2.70×10^{-3}
71	1.62×10^{-1}	1.56×10^{-1}	1.51×10^{-1}	1.02×10^{-2}	9.90×10^{-3}	8.30×10^{-3}
72	1.62×10^{-1}	1.56×10^{-1}	1.51×10^{-1}	7.10×10^{-3}	2.80×10^{-3}	2.60×10^{-3}
73	1.62×10^{-1}	1.56×10^{-1}	1.51×10^{-1}	1.14×10^{-2}	1.11×10^{-2}	1.00×10^{-2}
81	1.56×10^{-1}	1.28×10^{-1}	1.89×10^{-1}	9.70×10^{-3}	2.80×10^{-3}	2.40×10^{-3}
82	1.56×10^{-1}	1.28×10^{-1}	1.89×10^{-1}	2.40×10^{-3}	3.30×10^{-3}	2.60×10^{-3}
83	1.56×10^{-1}	1.28×10^{-1}	1.89×10^{-1}	2.20×10^{-3}	2.50×10^{-3}	5.80×10^{-3}
91	1.58×10^{-1}	1.70×10^{-1}	1.89×10^{-1}	4.20×10^{-3}	5.50×10^{-3}	3.50×10^{-3}
92	1.58×10^{-1}	1.70×10^{-1}	1.89×10^{-1}	1.70×10^{-3}	2.20×10^{-3}	1.70×10^{-3}
93	1.58×10^{-1}	1.70×10^{-1}	1.89×10^{-1}	4.60×10^{-3}	7.30×10^{-3}	4.90×10^{-3}

From the results obtained, the voltage threshold was set to 0.135 and the current threshold was set to 0.019. It can be seen from Figure 9 that relays 41, 42, 43, 61, 62 and 63 exceeded

the voltage threshold, and from Figure 10 that relays 42, 61 and 62 exceeded the current threshold. In this case, however, only relays 42 and 61 were tripped, as they had the largest difference between the current detail coefficients on each bus. Thanks to the developed protection algorithm, the unnecessary tripping of protection relay 62 was avoided as it was not responsible for protecting the transmission line that connected buses 4 and 6.

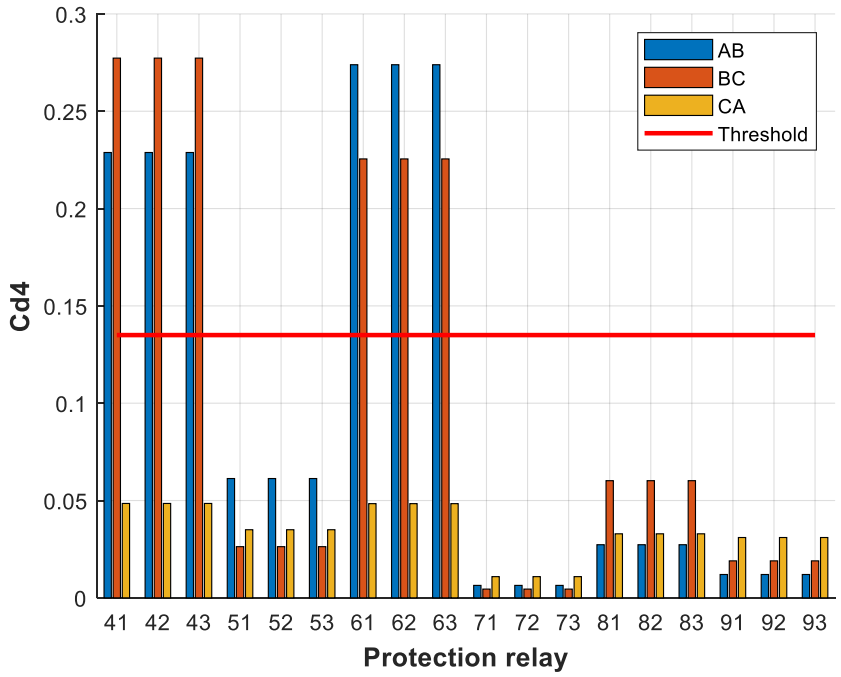

Figure 9. Differences in voltage Cd4-dB3 on the transmission line from bus 4 to bus 6.

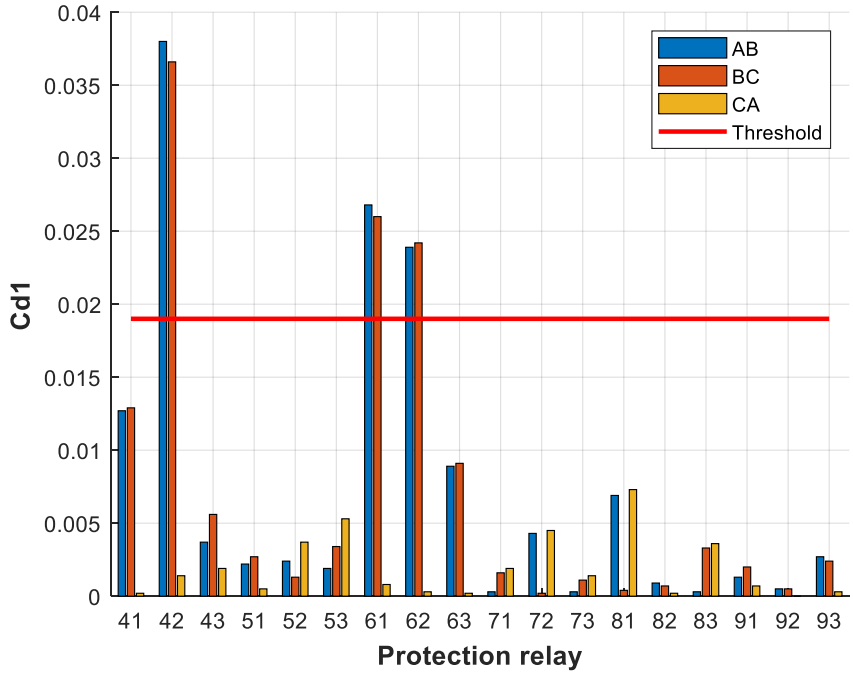

Figure 10. Differences in current Cd1-dB2 on the transmission line from bus 4 to bus 6.

7.3. Fault at Transmission Line from Bus 8 to Bus 9

In this case, a phase-to-ground arc fault was simulated in phase C of the transmission line, from bus 8 to bus 9 of the grid model. Table 4 below shows the values of the detail coefficients obtained for the voltage and current phases at each protection relay during the fault.

Table 4. Detail coefficients during phase-to-ground arc fault at transmission line from bus 8 to bus 9.

Relay No.	Detail Coefficients					
	Voltage (Cd4–dB3)			Current (Cd1–dB2)		
	Phase A	Phase B	Phase C	Phase A	Phase B	Phase C
41	1.52×10^{-1}	1.41×10^{-1}	1.92×10^{-1}	5.10×10^{-3}	5.90×10^{-3}	6.40×10^{-3}
42	1.52×10^{-1}	1.41×10^{-1}	1.92×10^{-1}	4.10×10^{-3}	4.80×10^{-3}	5.30×10^{-3}
43	1.52×10^{-1}	1.41×10^{-1}	1.92×10^{-1}	8.40×10^{-3}	8.10×10^{-3}	4.80×10^{-3}
51	7.16×10^{-2}	8.61×10^{-2}	1.14×10^{-1}	5.90×10^{-3}	1.80×10^{-3}	2.30×10^{-3}
52	7.16×10^{-2}	8.61×10^{-2}	1.14×10^{-1}	1.70×10^{-3}	1.50×10^{-3}	1.70×10^{-3}
53	7.16×10^{-2}	8.61×10^{-2}	1.14×10^{-1}	1.30×10^{-3}	1.40×10^{-3}	9.40×10^{-3}
61	1.04×10^{-1}	1.13×10^{-1}	9.08×10^{-2}	4.80×10^{-3}	2.20×10^{-3}	3.00×10^{-3}
62	1.04×10^{-1}	1.13×10^{-1}	9.08×10^{-2}	2.10×10^{-3}	2.00×10^{-3}	2.70×10^{-3}
63	1.04×10^{-1}	1.13×10^{-1}	9.08×10^{-2}	1.10×10^{-3}	1.10×10^{-3}	5.30×10^{-3}
71	1.76×10^{-1}	2.31×10^{-1}	2.00×10^{-1}	1.24×10^{-2}	9.80×10^{-3}	1.34×10^{-2}
72	1.76×10^{-1}	2.31×10^{-1}	2.00×10^{-1}	3.50×10^{-2}	6.20×10^{-3}	5.70×10^{-3}
73	1.76×10^{-1}	2.31×10^{-1}	2.00×10^{-1}	1.22×10^{-2}	2.35×10^{-2}	1.70×10^{-2}
81	1.64×10^{-1}	2.03×10^{-1}	3.30×10^{-1}	1.12×10^{-2}	5.80×10^{-3}	2.18×10^{-2}
82	1.64×10^{-1}	2.03×10^{-1}	3.30×10^{-1}	7.00×10^{-3}	6.90×10^{-3}	6.18×10^{-2}
83	1.64×10^{-1}	2.03×10^{-1}	3.30×10^{-1}	4.60×10^{-3}	5.40×10^{-3}	1.38×10^{-2}
91	2.30×10^{-1}	2.33×10^{-1}	7.05×10^{-1}	1.70×10^{-3}	1.70×10^{-3}	9.50×10^{-3}
92	2.30×10^{-1}	2.33×10^{-1}	7.05×10^{-1}	2.50×10^{-3}	1.80×10^{-3}	1.94×10^{-2}
93	2.30×10^{-1}	2.33×10^{-1}	7.05×10^{-1}	5.50×10^{-3}	2.80×10^{-3}	1.12×10^{-2}

Now from the results obtained, the voltage threshold was set to 0.24 and the current threshold was set to 0.028. From Figure 11, relays 91, 92 and 93 exceeded the voltage threshold, and from Figure 12, it is seen that only relay 82 exceeded the current threshold. In this case, only relays 82 and 92 were tripped as they registered the largest difference between the current detail coefficients for each bus.

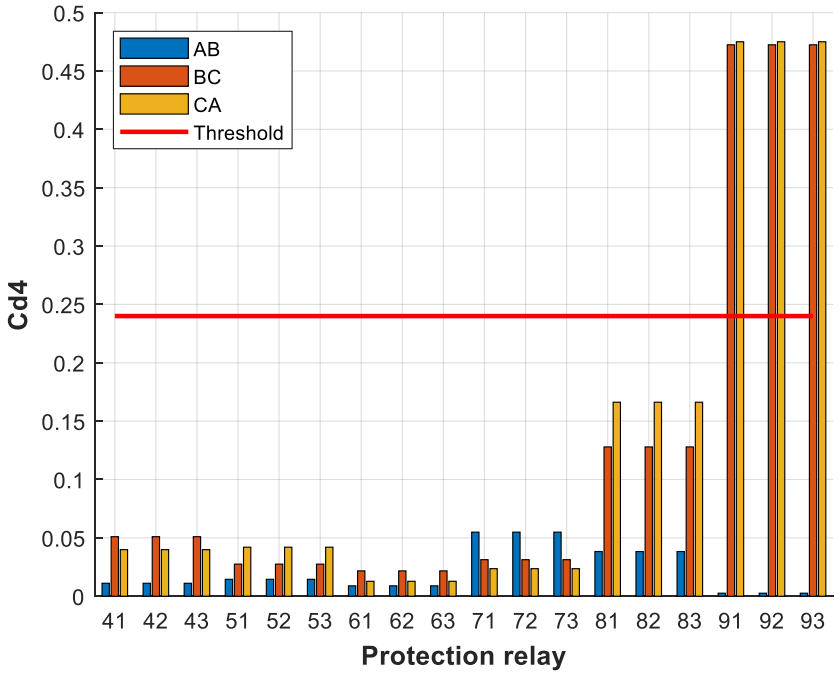

Figure 11. Differences in the voltage Cd4-dB3 on the transmission line from bus 8 to bus 9.

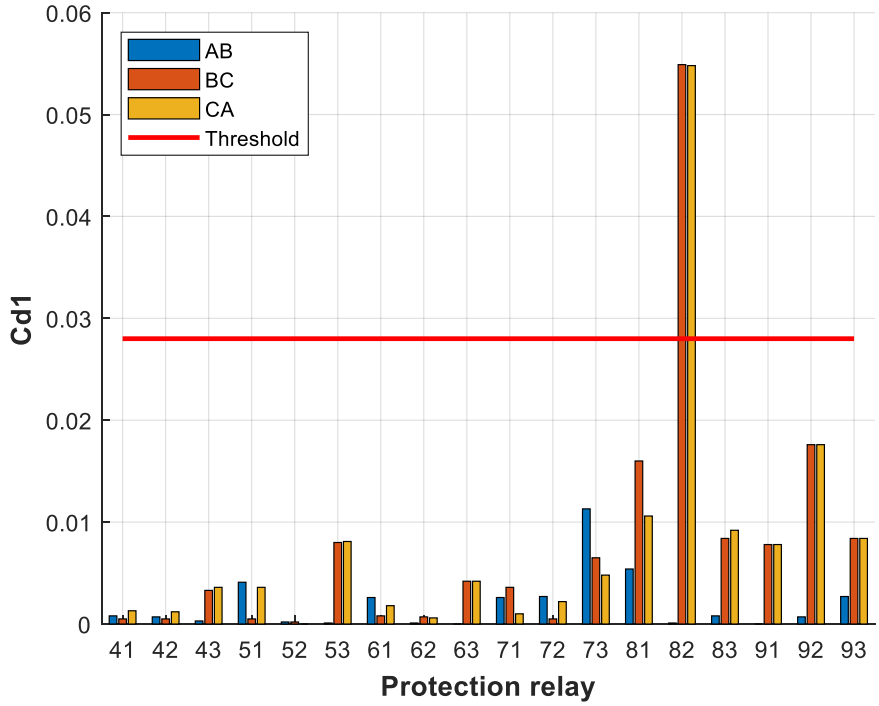

Figure 12. Differences in the current Cd1-dB2 on the transmission line from bus 8 to bus 9.

8. Conclusions

In this paper, a new protection technique was presented that solves the problems of detecting ground faults due to the low fault current contribution of grid-forming power converters in an electrical power system with 100% converter-interface-based generation. To develop this technique, the IEEE nine-bus test system was used to reproduce the behavior of a grid with 100% renewable energy sources, which are based on power electronic interfaces. A complete grid-forming VSC model was designed to replicate the role of grid sources in an electrical power system. In addition, an arc ground fault scheme was modelled using the IEEE nine-bus system to simulate a realistic electrical fault scenario.

The protection algorithm performed a wavelet transform analysis to decompose the voltage and current waveforms measured where the protection relays are installed. Once the detail coefficients have been obtained, the protection algorithm processes and analyses them to detect ground faults, providing full selectivity in the identification of the faulty transmission line. The results of a simulation show that the proposed protection technique operates reliably under different ground fault scenarios; this is because the wavelet transform analysis makes it possible to detect singularities in high and low frequency voltage and current signals and allows them to be classified in terms of time and magnitude when they occur. The differences between the nominal load current and fault current are in the range of 1 p.u., whereas the detail coefficients provide differences of up to 10 p.u. In this way, the problems with sensitivity and selectivity that prevent actual protection relays from detecting ground faults with low current contribution are solved.

In addition, currently installed protection relays to protect transmission lines are usually segregated line differential relays, distance relays and directional ground fault relays whose minimum tripping times are not usually less than 30 ms. Thanks to the use of the wavelet transform, the ground fault detection times do not exceed one complete cycle, so the tripping time of the new proposed method will not exceed the tripping times of the currently installed protection systems.

Based on the results and experience obtained from the application of this wavelet transform to fault detection, generalized configurations cannot be established for all cases and applications, and a rigorous depth study is, therefore, required for each scenario to choose the best wavelet configuration. Future work will focus on phase-to-phase faults,

multiple generation technologies and real-time tests of the algorithm with hardware-in-the-loop tools.

Author Contributions: Conceptualization, R.G. and S.A.; methodology, L.S.A.G.; software, L.S.A.G.; validation, R.G. and S.A.; formal analysis, L.S.A.G.; investigation, L.S.A.G., R.G. and S.A.; resources, R.G. and S.A.; writing—original draft preparation, L.S.A.G.; writing—review and editing, R.G. and S.A.; supervision, R.G. and S.A. All authors have read and agreed to the published version of the manuscript.

Funding: This work was supported by the Autonomous Community of Madrid under the PROMINT—CM project (S2018/EMT-4366).

Data Availability Statement: Not applicable.

Conflicts of Interest: The authors declare no conflict of interest.

References

1. Plet, C.A.; Graovac, M.; Green, T.C.; Iravani, R. Fault response of grid-connected inverter dominated networks. In Proceedings of the IEEE PES General Meeting, Minneapolis, MN, USA, 25–29 July 2010; pp. 1–8. [CrossRef]
2. Dolado, J.; Amenedo, J.L.R.; Arnaltes, S.; Eloy-Garcia, J. Improving the Inertial Response of a Grid-Forming Voltage Source Converter. *Electronics* **2022**, *11*, 2303. [CrossRef]
3. Jia, J.; Yang, G.; Nielsen, A.H. A Review on Grid-Connected Converter Control for Short-Circuit Power Provision under Grid Unbalanced Faults. *IEEE Trans. Power Deliv.* **2018**, *33*, 649–661. [CrossRef]
4. Manson, S.; McCullough, E. Practical Microgrid Protection Solutions: Promises and Challenges. *IEEE Power Energy Mag.* **2021**, *19*, 58–69. [CrossRef]
5. Reno, M.J.; Brahma, S.; Bidram, A.; Ropp, M.E. Influence of Inverter-Based Resources on Microgrid Protection: Part 1: Microgrids in Radial Distribution Systems. *IEEE Power Energy Mag.* **2021**, *19*, 36–46. [CrossRef]
6. Vegunta, S.C.; Higginson, M.J.; Kenarangui, Y.E.; Li, G.T.; Zabel, D.W.; Tasdighi, M.; Shadman, A. AC Microgrid Protection System Design Challenges—A Practical Experience. *Energies* **2021**, *14*, 2016. [CrossRef]
7. Brahma, S.M.; Girgis, A.A. Development of Adaptive Protection Scheme for Distribution Systems With High Penetration of Distributed Generation. *IEEE Trans. Power Deliv.* **2004**, *19*, 56–63. [CrossRef]
8. Brucoli, M.; Green, T.C.; McDonald, J.D.F. Modelling and analysis of fault behaviour of inverter microgrids to aid future fault detection. In Proceedings of the 2007 IEEE International Conference on System of Systems Engineering, San Antonio, TX, USA, 16–18 April 2007. [CrossRef]
9. Brucoli, M. *Fault Behaviour and Fault Detection in Islanded Inverter-Only Microgrids*; Imperial College London: London, UK, 2008.
10. Zamani, M.A.; Sidhu, T.S.; Yazdani, A. A protection strategy and microprocessor-based relay for low-voltage microgrids. *IEEE Trans. Power Deliv.* **2011**, *26*, 1873–1883. [CrossRef]
11. Mohamed, N.A.; Salama, M.M.A. A review on the proposed solutions to microgrid protection problems. In Proceedings of the 2016 IEEE Canadian Conference on Electrical and Computer Engineering (CCECE), Vancouver, BC, Canada, 15–18 May 2016; Volume 2016, pp. 1–5. [CrossRef]
12. Mirsaeidi, S.; Said, D.M.; Mustafa, M.W.; Habibuddin, M.H.; Miveh, M.R. A comprehensive overview of different protection schemes in micro-grids. *Int. J. Emerg. Electr. Power Syst.* **2013**, *14*, 327–332. [CrossRef]
13. Chen, Z.; Pei, X.; Yang, M.; Peng, L.; Shi, P. A Novel Protection Scheme for Inverter-Interfaced Microgrid (IIM) Operated in Islanded Mode. *IEEE Trans. Power Electron.* **2018**, *33*, 7684–7697. [CrossRef]
14. Oureilidis, K.O.; Demoulias, C.S. A Fault Clearing Method in Converter-Dominated Microgrids with Conventional Protection Means. *IEEE Trans. Power Electron.* **2016**, *31*, 4628–4640. [CrossRef]
15. Sortomme, E.; Venkata, S.S.; Mitra, J. Microgrid protection using communication-assisted digital relays. *IEEE Trans. Power Deliv.* **2010**, *25*, 2789–2796. [CrossRef]
16. Huang, W.; Nengling, T.; Zheng, X.; Fan, C.; Yang, X.; Kirby, B.J. An impedance protection scheme for feeders of active distribution networks. *IEEE Trans. Power Deliv.* **2014**, *29*, 1591–1602. [CrossRef]
17. Yabe, K. Power differential method for discrimination between fault and magnetizing inrush current in transformers. *IEEE Trans. Power Deliv.* **1997**, *12*, 1109–1115. [CrossRef]
18. Gilany, M.; Al-Kandari, A.M.; Madouh, J.Y. A new strategy for determining fault zones in distance relays. *IEEE Trans. Power Deliv.* **2008**, *23*, 1857–1863. [CrossRef]
19. Farkhani, J.S.; Zareein, M.; Najafi, A.; Melicio, R. The Power System and Microgrid Protection—A Review. *Appl. Sci.* **2020**, *10*, 8271. [CrossRef]
20. Arrabé, R.G. *New Methods and Protection Systems for AC and DC Power Networks*; Universidad Politécnica de Madrid: Madrid, Spain, 2018.
21. Qoria, T.; Gruson, F.; Colas, F.; Kestelyn, X.; Guillaud, X. Current limiting algorithms and transient stability analysis of grid-forming VSCs. *Electr. Power Syst. Res.* **2020**, *189*, 106726. [CrossRef]

22. Huang, L.; Xin, H.; Wang, Z.; Zhang, L.; Wu, K.; Hu, J. Transient Stability Analysis and Control Design of Droop-Controlled Voltage Source Converters Considering Current Limitation. *IEEE Trans. Smart Grid* **2019**, *10*, 578–591. [CrossRef]
23. Gkountaras, A.; Dieckerhoff, S.; Sezi, T. Evaluation of current limiting methods for grid forming inverters in medium voltage microgrids. In Proceedings of the 2015 IEEE Energy Conversion Congress and Exposition (ECCE), Montreal, QC, Canada, 20–24 September 2015; pp. 1223–1230. [CrossRef]
24. Wu, H.; Li, X.; Stade, D.; Schau, H. Arc fault model for low-voltage AC systems. *IEEE Trans. Power Deliv.* **2005**, *20*, 1204–1205. [CrossRef]
25. Parizad, A.; Baghaee, H.R.; Tavakoli, A.; Jamali, S. Optimization of f Arc Models Parameter s Using Genetic Algorithm. In Proceedings of the 2009 International Conference on Electric Power and Energy Conversion Systems, (EPECS), Sharjah, United Arab Emirates, 10–12 November 2009; pp. 1–7.
26. CKim, H.; Kim, H.; Ko, Y.H.; Byun, S.H.; Aggarwal, R.K.; Johns, A.T. A novel fault-detection technique of high-impedance arcing faults in transmission lines using the wavelet transform. *IEEE Trans. Power Deliv.* **2002**, *17*, 921–929. [CrossRef]
27. Angrisani, L.; Daponte, P.; D'Apuzzo, M.; Testa, A. A measurement method based on the wavelet transform for power quality analysis. *IEEE Trans. Power Deliv.* **1998**, *13*, 990–998. [CrossRef]
28. Poisson, O.; Rioual, P.; Meunier, M. Detection and measurement of power quality disturbances using wavelet transform. *IEEE Trans. Power Deliv.* **2000**, *15*, 1039–1044. [CrossRef]
29. Reddy, V.M.; Rao, S.S.; Mercede, F.J. On the use of wavelets for the detection and analysis of power system transients. In Proceedings of the IEEE Power Engineering Society, 1999 Winter Meeting, New York, NY, USA, 1 January–4 February 1999; Volume 2, pp. 1293–1299. [CrossRef]
30. Magnago, F.H.; Abur, A. Fault location using wavelets. *IEEE Trans. Power Deliv.* **1998**, *13*, 1475–1480. [CrossRef]
31. Bhattacharjee, P.P. Application of wavelets to model short-term power system disturbances. *IEEE Trans. Power Syst.* **1996**, *11*, 2031–2037. [CrossRef]
32. Yu, R.; Fu, Z.; Wang, Q.; Sun, S.; Chen, H.; Xu, Q.; Chen, X. Modeling and simulation analysis of single phase arc grounding fault based on MATLAB. In Proceedings of the International Conference on Electronic & Mechanical Engineering & Information Technology, EMEIT, Harbin, China, 12–14 August 2011; Volume 9, pp. 4607–4610. [CrossRef]
33. Pérez, F.E.; Aguilar, R.; Orduna, E.; Jäger, J.; Guidi, G. High-speed non-unit transmission line protection using single-phase measurements and an adaptive wavelet: Zone detection and fault classification. *IET Gener. Transm. Distrib.* **2012**, *6*, 593–604. [CrossRef]
34. Jung, H.; Park, Y.; Han, M.; Lee, C.; Park, H.; Shin, M. Novel technique for fault location estimation on parallel transmission lines using wavelet. *Int. J. Electr. Power Energy Syst.* **2007**, *29*, 76–82. [CrossRef]
35. Khan, F.A.; Shees, M.M.; Alsharekh, M.F.; Alyahya, S.; Saleem, F.; Baghel, V.; Sarwar, A.; Islam, M.; Khan, S. Open-circuit fault detection in a multilevel inverter using sub-band wavelet energy. *Electronics* **2022**, *11*, 123. [CrossRef]
36. Meliopoulos, A.P.S.; Lee, C.-H. An alternative method for transient analysis via wavelets. *IEEE Trans. Power Deliv.* **2000**, *15*, 114–121. [CrossRef]
37. Robertson, D.C.; Camps, O.I.; Mayer, J.S.; Gish, W.B. Wavelets and electromagnetic power system transients. *IEEE Trans. Power Deliv.* **1996**, *11*, 1050–1056. [CrossRef]
38. Santoso, S.; Powers, E.J.; Grady, W.M.; Hofmann, P. Power quality assessment via wavelet transform analysis. *IEEE Trans. Power Deliv.* **1996**, *11*, 924–930. [CrossRef]